View metadata, citation and similar papers at core.ac.uk

brought to you by CORE

provided by Elsevier - Publisher Connector

Biochimica et Biophysica Acta 1848 (2015) 1563–1572

Contents lists available at ScienceDirect

Biochimica et Biophysica Acta

journal homepage: www.elsevier.com/locate/bbamem

Functional characterization of the organic cation transporters (OCTs) in human airway pulmonary epithelial cells

Filippo Ingoglia [a,1], Rossana Visigalli [a,1], Bianca Maria Rotoli [a], Amelia Barilli [a], Benedetta Riccardi [b], Paola Puccini [b], Valeria Dall'Asta [a,*]

[a] Dept. of Biomedical, Biotechnological and Translational Sciences (SBiBiT), University of Parma, Via Volturno 39, 43125 Parma, Italy
[b] Preclinical Pharmacokinetics, Biochemistry & Metabolism Dept., Chiesi Farmaceutici, Largo F. Belloli 11/A, 43122 Parma, Italy

ARTICLE INFO

Article history:
Received 16 October 2014
Received in revised form 25 March 2015
Accepted 2 April 2015
Available online 13 April 2015

Keywords:
Pulmonary epithelium
Organic cation transporters
OCT1
OCT2
OCT3
Cationic drug transporters

ABSTRACT

Organic cation transporters (OCT1–3) mediate the transport of organic cations including inhaled drugs across the cell membrane, although their role in lung epithelium hasn't been well understood yet. We address here the expression and functional activity of OCT1–3 in human airway epithelial cells A549, Calu-3 and NCI-H441. Kinetic and inhibition analyses, employing [^{3}H]1-methyl-4-phenylpyridinium (MPP+) as substrate, and the compounds quinidine, prostaglandine E2 (PGE_2) and corticosterone as preferential inhibitors of OCT1, OCT2, and OCT3, respectively, have been performed. A549 cells present a robust MPP+ uptake mediated by one high-affinity component (K_m ~ 50 μM) which is identifiable with OCT3. Corticosterone, indeed, completely inhibits MPP+ transport, while quinidine and PGE_2 are inactive and SLC22A3/OCT3 silencing with siRNA markedly lowers MPP+ uptake. Conversely, Calu-3 exhibits both a high (K_m < 20 μM) and a low affinity (K_m > 0.6 mM) transport components, referable to OCT3 and OCT1, respectively, as demonstrated by the inhibition analysis performed at proper substrate concentrations and confirmed by the use of specific siRNA. These transporters are active also when cells are grown under air–liquid interface (ALI) conditions. Only a very modest saturable MPP+ uptake is measurable in NCI-H441 cells and the inhibitory effect of quinidine points to OCT1 as the subtype functionally involved in this model. Finally, the characterization of MPP+ transport in human bronchial BEAS-2B cells suggests that OCT1 and OCT3 are operative. These findings could help to identify *in vitro* models to be employed for studies concerning the specific involvement of each transporter in drug transportation.

© 2015 Elsevier B.V. All rights reserved.

1. Introduction

Membrane transporters are known to have a significant impact on the absorption and elimination of a large number of drugs, determining their pharmacokinetic profiles, safety and efficacy [1]. A large family of transporters are the Solute Link Carrier, SLC22A, which are often found in epithelial membranes where they mediate uptake and secretion of organic cations [2]. SLC22A gene family includes electrogenic transporters (*i.e.* OCT1/SLC22A1, OCT2/SLC22A2, and OCT3/SLC22A3) and pH-dependent novel transporters, namely OCTN1/SLC22A4 and OCTN2/SLC22A5 [3]. Although OCTNs may mediate the transport of cationic chemicals, they are most notably known for their ability to mediate the influx of carnitine, and several mutations in the SLC22A5 gene have been identified in patients with primary carnitine deficiency [4]. OCTs are involved in the bidirectional translocation of small (<500 Da) organic cations across the cell membrane. They are endowed with broad, overlapping affinities for a wide range of substrates, including endogenous molecules, such as choline, creatinine and neurotransmitters [5], as well as a variety of xenobiotics [6]. The model substrates for the functional study of OCTs are tetraethylammonium (TEA) and the most specific neurotoxin methyl 4-phenylpiridinium (MPP+) [5,7]. None of the substrates thus far employed interacts only with a single OCT transporter, as demonstrated employing transfected cell models, such as CHO [8], HEK293 [9,10] or xenopus oocytes [11–13]. In non transfected cell models the characterization of OCT transport activity appears further complicated by the lack of specific inhibitors too [5]. The study of OCT transporters has been mainly focused on liver, kidneys, intestine and blood–brain barrier, with the lung remaining largely unchartered terrain, despite its pharmacological relevance [14,15]. Actually, the lung offers a great potential as a portal into the systemic circulation for drugs endowed with difficult oral pharmacokinetics or stability issue. Moreover, since several common inhaled drugs, positively charged at physiological pH, have been reported to interact with OCT [16], the role of these transporters in lung epithelium

Abbreviations: ALI, air–liquid interface culture; EBSS, Earle's Balanced Salt Solution; MPP+, 1-methyl-4-phenylpyridinium; OCT, organic cation transporter; PBS, phosphate-buffered saline solution; PGE_2, prostaglandine E_2; TEER, transepithelial electrical resistance

* Corresponding author at: Unità di Patologia Generale, Dipartimento di Scienze Biomediche, Biotecnologiche e Traslazionali (SBiBiT), Università degli Studi di Parma, Via Volturno, 39, 43125 Parma, Italy. Tel.: +39 0521 033787; fax: +39 0521 033742.
E-mail address: valeria.dallasta@unipr.it (V. Dall'Asta).

[1] F.I. and R.V. equally contributed to this work.

http://dx.doi.org/10.1016/j.bbamem.2015.04.001
0005-2736/© 2015 Elsevier B.V. All rights reserved.

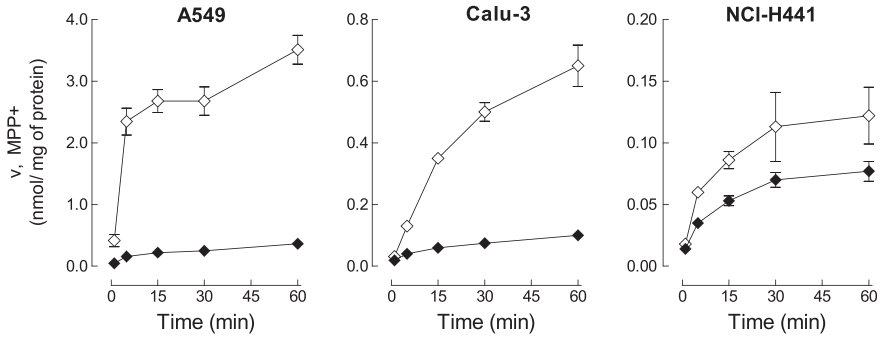

Fig. 1. Time-dependent accumulation of MPP+ in A549, Calu-3 and NCI-H441 cells. Cells were incubated for the indicated times in the transport buffer (see section Material and methods) containing [^{3}H]MPP+ (10 μM; 2 μCi/ml) (open symbols). Non-specific binding of the substrate was estimated by measuring [^{3}H]MPP+ uptake in the presence of an excess of unlabelled substrate (2 mM) (filled symbols). Each point represents the mean ± S.D. of four independent determinations. The experiments have been repeated three times with comparable results.

(especially bronchiolar and alveolar systems) deserves particular attention. Evidence is now emerging that OCTs are involved in transport processes in various cell types of the lung [17,18], and differential expression of the transporters has been highlighted in cell models from different regions [19]. The aim of our study is to identify optimal cell models for studies concerning cationic drug absorption through OCTs in the airways. Thus far, the characterization of OCT-mediated transport in respiratory cell models has been performed employing the fluorescent cation Asp+ as substrate [16,20]. However, since also the choice of the substrate is known to influence the profile of inhibition of OCT-mediated uptake both quantitatively and qualitatively [21], it is conceivable that the use of substrates other than Asp+ may broaden the knowledge about OCT function. In this study we thoroughly characterize OCT transport activity in *in vitro* models of respiratory epithelium (alveolar A549, bronchial Calu-3, and distal lung NCI-H441 carcinoma cells, as well as in bronchial BEAS-2B cells) by means of an integrated approach combining data of mRNA expression with the kinetic and inhibition analyses of MPP+ transport.

2. Material and methods

2.1. Cell cultures

Calu-3, A549, NCI-H441 and BEAS-2B cell lines were obtained from American Type Culture Collection (ATCC, Rockville, MD, USA). Alveolar carcinoma A549 and immortalized BEAS-2B bronchial epithelial cells were cultured in Dulbecco's Modified Eagle Medium (DMEM, high glucose) supplemented with sodium pyruvate (1 mM). NCI-H441, originally derived from lung papillary adenocarcinoma, were cultured in RPMI-1640 (ATCC) and used at passages 36–41. Calu-3 cells, deriving from a human lung adenocarcinoma, were cultured in Eagle's Minimum Essential Medium (EMEM) supplemented with sodium pyruvate (1 mM) and used at passages 45–53. For all cell models, growth medium was supplemented with 10% fetal bovine serum (FBS) and 1% Penicillin/Streptomycin. Cell cultures were routinely cultured under physiological conditions (37.5 °C, 5% CO_2, 95% humidity) in 10-cm diameter dishes.

For growth under air–liquid interfaced culture (ALI) conditions, Calu-3 cells were initially seeded on Cell Culture Inserts (12 mm in diameter, pore size 0.4 μm; Falcon) at the density of 75×10^3 cells/well, with apical and basolateral fluid volumes corresponding to 250 and 700 μl, respectively. After 24 h, the apical fluid was completely removed, and the medium in the basolateral compartment was renewed every other day. Cell cultures were employed after 21 days, when the cell monolayers exhibited "tight" barrier properties, as represented by high transepithelial electrical resistance (TEER > 500 Ohm/cm^2, measured with an epithelial voltmeter (EVOM, World Precision Instruments, FL, USA)). The integrity of cell monolayers was preserved after the experiments.

2.2. qRT-polymerase chain reaction

For the analysis of mRNA expression 1 μg of total RNA, extracted with GenElute Mammalian Total RNA Miniprep Kit (Sigma Aldrich), was reverse-transcribed, and 40 ng of cDNA was amplified as described previously [22]. The following forward and reverse primers were employed: 5′ TGT CAC CGA AAA GCT GAG CC 3′ and 5′ TCC GTG AAC CAC AGG TAC ATC 3′ for SLC22A1/OCT1; 5′ CAT CGT CAC CGC GTT TAA CCT G 3′ and 5′ AGC CGA TAC TCA TAG AGC CAA T 3′ for SLC22A2/OCT2; 5′ AGG TAT GGC AGG ATC GTC ATT 3′ and 5′ GCA GGA AGC GGA AGA TCA CA 3′ for SLC22A3/OCT3; 5′ GCA GCC ATC AGG TAA GCC AAG 3′ and 5′ AGC GGA CCC TCA GAA GAA AGC 3′ for the housekeeping RPL15 (Ribosomal Protein Like 15). The expression

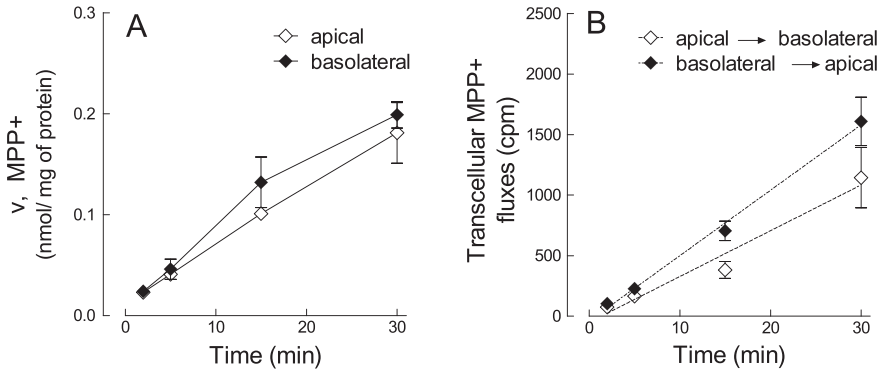

Fig. 2. MPP+ fluxes in Calu-3 ALI. Monolayers of polarized Calu-3 cells grown in air–liquid interface conditions (ALI) were incubated for the indicated time in the transport buffer containing [^{3}H]MPP+ (10 μM; 2 μCi/ml), either added at the apical or at the basolateral side, as indicated. The intracellular MPP+ accumulation (panel A) and the transcellular fluxes of MPP+ (panel B) were determined as described in the section Material and methods. Each point represents the mean ± S.D. of three independent determinations. The experiments have been repeated twice with comparable results.

of the gene of interest under each experimental condition was normalized to that of the housekeeping gene and shown relatively to its expression level in a reference sample (=1), as indicated.

2.3. siRNA transfection

Short interfering RNA (siRNA) analysis of SLC22A1/OCT1 and SLC22A3/OCT3 was performed employing specific FlexiTube siRNA (Cat.# 1027416) by Qiagen® (Milano, Italy), according to Fast-Forward Transfection protocol provided by the manufacturer. Briefly, cells (1×10^5/ml) were transfected by adding to 1 ml of cell suspension 200 μl of serum free RPMI containing HiPerFect Transfection Reagent (9 μl) and 100 nM AllStar Negative Control siRNA (Cat.# SI03650318; scrambled) or 25 nM each of 4 different OCT1 (Cat. # SI04193539, SI04205390, SI4270483, SI04318811) or OCT3 siRNA (Cat. # SI00721357, SI04140598, SI04159848, SI04218935). Transfected cells were seeded as required by the experimental plan, and maintained under growing conditions for 96 h. Control, untransfected cells were also cultured in parallel.

2.4. Uptake studies

For uptake assay, 3×10^4 cells were seeded onto 96-well trays (Falcon) and uptake was measured when the confluence was reached. Activity of OCTs was determined by measuring the uptake of the radiolabeled substrate [^{3}H]1-methyl-4-phenylpyridinium (MPP+). After two rapid washes in prewarmed transport buffer (Earle's Balanced Salt Solution (EBSS) containing (in mM) 117 NaCl, 1.8 $CaCl_2$, 5.3 KCl, 0.9 NaH_2PO4, 0.8 $MgSO_4$, 5.5 glucose, 26 TRIS–HCl adjusted to pH 7.4), cells were incubated in transport buffer containing [^{3}H]MPP^+ (2 μCi/ml) for the times detailed in each experiment (see figure legends). For the determination of sodium-independent MPP+ uptake, a modified EBSS in which NaCl was replaced with equimolar *N*-methylglucamine. When required, the inhibitors (corticosterone, prostaglandine E_2 and quinidine) were in the transport buffer at the indicated concentrations. At the indicated times, transport buffer containing the radiolabeled substrate was removed, and the experiment was terminated by two rapid washes (<10 s) in ice-cold 300 mM urea. Cell monolayers were extracted in ethanol and the radioactivity in cell extracts was determined with Wallac Microbeta Trilux^2 liquid scintillation spectrometer (Perkin Elmer, Monza, Italy). Protein content was determined directly in the well using a modified Lowry procedure [23]. MPP+ uptake is expressed as nmol/mg of protein. No relevant difference in transport rates was observed among cells at different passage number.

The apparent kinetic parameters K_m (Michaelis constant) and V_{max} (maximum transport rate) of MPP+ uptake were calculated by nonlinear regression fitting according to the following Michaelis–Menten equations:

$$v = \frac{V_{max} \times [S]}{K_m + [S]} + K_d \times [S] \quad (1)$$

for a single saturable component plus diffusion, where v is the initial influx, V_{max} is the maximal influx, K_m is the Michaelis constant and K_d is the diffusion constant;

$$v = \frac{V_{max1} \times [S]}{K_{m1} + [S]} + \frac{V_{max2} \times [S]}{K_{m2} + [S]} + K_d \times [S] \quad (2)$$

for two saturable transport components plus diffusion, where the indices 1 and 2 indicate the high- and low-affinity components, respectively.

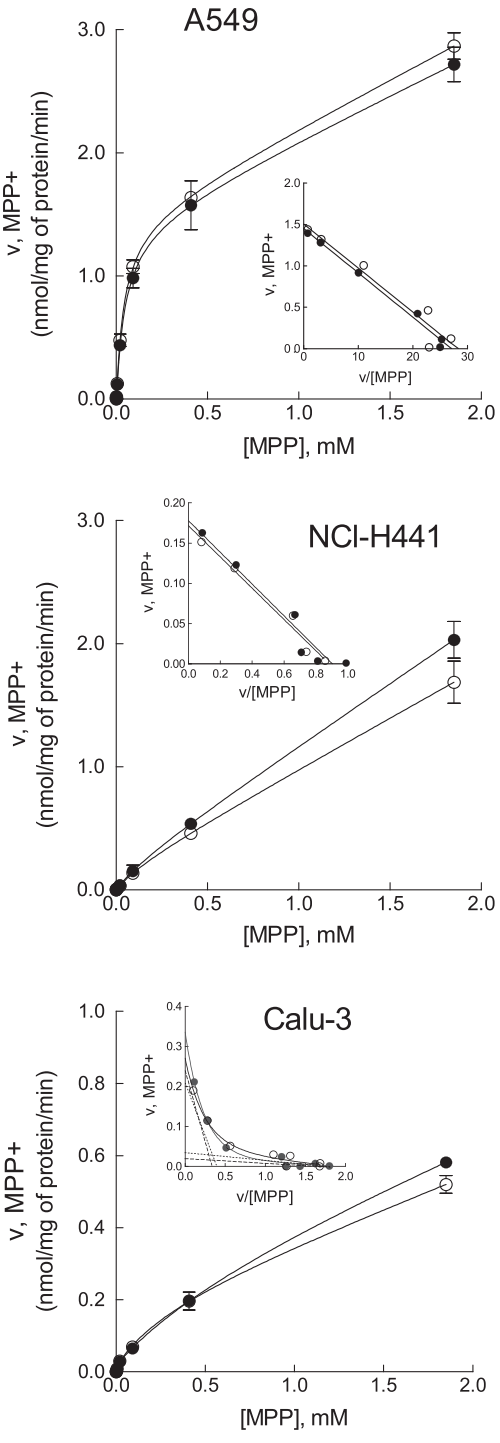

Fig. 3. Kinetic analysis of MPP+ uptake. A549, NCl-H441 and Calu-3 cells were incubated in the presence of the indicated concentrations (from 0.8 to 1850 μM) of [^{3}H]MPP+ (2 μCi/ml) for 5 min (A549), 10 min (Calu-3) or 15 min (NCl-H441), in the absence (open symbols) or in the presence (filled symbols) of Na^+. Nonlinear fitting of the data was performed employing Eq. (1) (A549 and NCl-H441 cells) or Eq. (2) (Calu-3 cells) (see section Material and methods). The resulting kinetic constants are given in Table 1. Inserts in each graph show the Eadie–Hofstee transformations of the saturable uptake (obtained after subtraction of the diffusive component estimated by the nonlinear fitting). Straight lines are drawn employing the values of the kinetic parameters given by nonlinear regression (see Table 1). Curves for Calu-3 represent the nonlinear fitting of the data. Points are mean ± S.D. of three independent determinations. The experiment has been repeated twice with comparable results.

Table 1
Kinetic parameters describing the uptake of MPP+.
Data are estimated from nonlinear regression analysis shown in Fig. 3.

		High affinity		Low affinity	
		Km1 mM	Vmax1 nmol/mg of protein/min	Km2 mM	Vmax2 nmol/mg of protein/min
A549	Na^+-present	0.050 ± 0.0015	1.433 ± 0.016		
	Na^+-absent	0.043 ± 0.0019	1.471 ± 0.022		
NCl-H441	Na^+-present	0.184 ± 0.018	0.178 ± 0.009		
	Na^+-absent	0.176 ± 0.0138	0.172 ± 0.007		
Calu-3	Na^+-present	0.014 ± 0.005	0.025 ± 0.005	0.78 ± 0.08	0.269 ± 0.017
	Na^+-absent	0.020 ± 0.004	0.038 ± 0.004	0.60 ± 0.04	0.240 ± 0.023

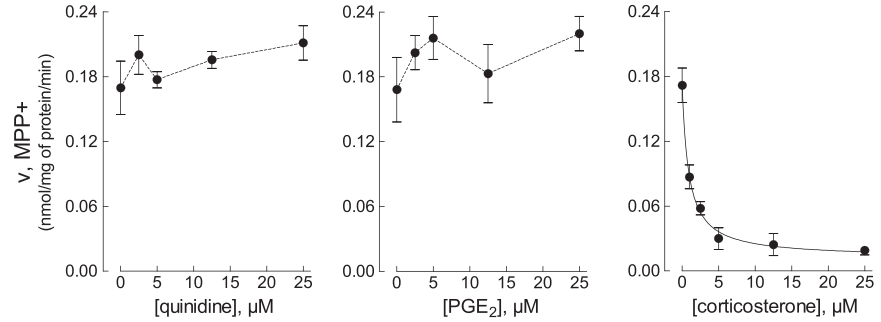

Fig. 4. Inhibition of MPP+ uptake in A549 cells. A549 cells were incubated for 5 min in the transport buffer containing [^{3}H]MPP+ (5 μM; 2 μCi/ml) with the indicated concentrations of inhibitors. Each point represents the mean ± S.D. of four independent determinations. For corticosterone, data were fitted by Eq. (3) (see section Material and methods). The experiment has been repeated three times with comparable results.

The following equation was employed to describe the effects of inhibitors on MPP+ uptake:

$$v = \frac{V_0 - I_{max} \times [I]}{[I]_{0.5} + [I]} \quad (3)$$

where v is the initial influx, v_0 is the uptake in the absence of the inhibitor, I_{max} is the maximal inhibition, and $[I]_{0.5}$ is the inhibitor concentration required for half-maximal inhibition. The *Ki* value was calculated from $[I]_{0.5}$ employing the following equation:

$$[I]_{0.5} = \left(1 + \frac{[S]}{Km}\right) \times Ki \quad (4)$$

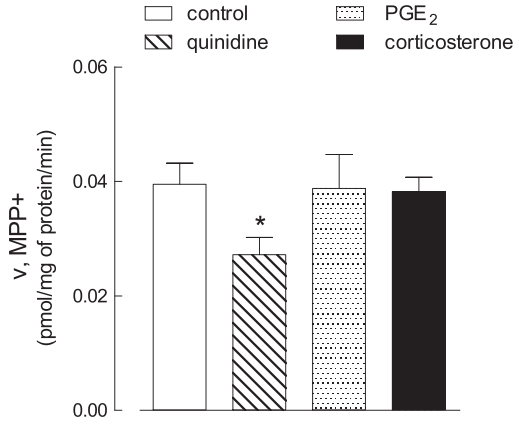

Fig. 5. Inhibition of MPP+ uptake in NCl-H441 cells. NCl-H441 cells were incubated for 15 min in the transport buffer containing [^{3}H]MPP+ (50 μM; 2 μCi/ml) in the absence (control) and in the presence of the indicated inhibitors (250 μM). Bars represent the mean ± S.D. of four independent determinations. The experiments have been repeated three times with comparable results. *$p < 0.05$ vs control.

2.5. Determination of MPP+ fluxes in polarized Calu-3

Cell monolayers, cultured on permeable supports (Cell Culture Insert, Falcon), were washed once with EBSS. For the determination of apical and basolateral uptake, 50 or 600 μl of EBSS containing [^{3}H]MPP$^+$ (10 μM, 2 μCi) was added to the apical or basolateral compartment, respectively, while the opposite compartment was incubated in EBSS. For the determination of transcellular fluxes, aliquots of the solution in the opposite compartment were collected and the radioactivity was measured with a Wallac Microbeta Trilux^2 liquid scintillation spectrometer. To determine the intracellular accumulation of the substrate, the porous membranes were rapidly washed in 300 mM ice-cold urea, then detached from the culture inserts. Cell monolayers were extracted in 0.2 ml ethanol and the radioactivity of cell extracts was measured with Wallac Microbeta Trilux^2 liquid scintillation spectrometer. Cell monolayers were then dissolved with 0.5% sodium deoxycholate in 1 M NaOH, and protein content was determined using a modified Lowry procedure, as described previously [23].

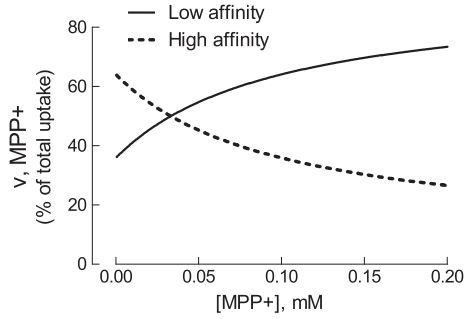

Fig. 6. Estimated relative contribution of low and high affinity components to MPP+ transport in Calu-3 cells. The curves have been calculated on the basis of the kinetic parameters presented in Table 1.

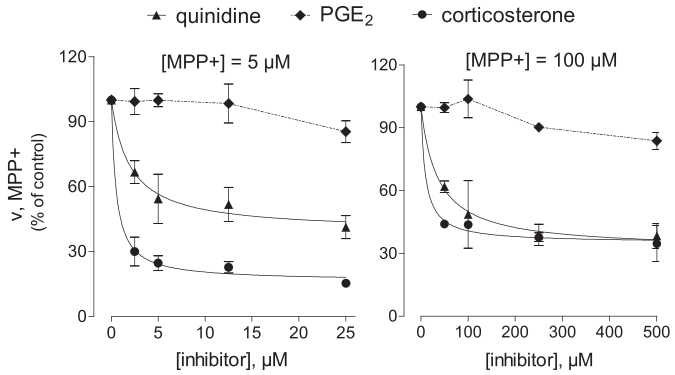

Fig. 7. Inhibition of MPP+ uptake in Calu-3 cells. Cells were incubated for 10 min in the transport buffer containing 5 μM (panel A) or 100 μM (panel B) [^{3}H]MPP+ (2 μCi/ml) in the presence of the indicated concentrations of the inhibitors. Data are expressed as percent of control (absence of inhibitor). Data were fitted by Eq. (3) (see section Material and methods). Each point represents the mean ± S.D. of four independent determinations. The experiment has been repeated three times with comparable results.

2.6. Data calculation and statistical analysis

Curve fittings were obtained employing Prism® 5.0 software (GraphPad, San Diego, CA). Unless otherwise stated, all experiments were performed in quadruplicate and data presented as mean ± SD. Statistical analysis was done with Prism® 5.0 software, using one-way ANOVA followed by Bonferroni post-hoc test.

2.7. Materials

Fetal bovine serum was purchased from EuroClone (Milano, Italy). Culture media for NCl-H441 were purchased from (ATCC, Rockville, MD, USA). Methyl-4-phenylpyridinium iodide, 1-[methyl-^{3}H], 85 Ci/mmol, was from ARC (American Radiolabeled Chemicals, St. Luis, MO, USA) and was obtained from Bcs Biotech (Cagliari, Italy). Sigma-Aldrich was the source of the inhibitors, and, unless otherwise specified, of all other chemicals.

3. Results

3.1. Time-dependent accumulation of MPP+ in A549, Calu-3 and NCl-H441 cells

The uptake of 1-methyl-4-phenylpyridinium (MPP+) by the three cell lines has been preliminary measured at different times, up to 60 min (Fig. 1). In A549 MPP+ uptake was linear up to 5 min incubation, while in Calu-3 cells linearity was maintained up to 15 min. MPP+ uptake was completely abolished by an excess of unlabelled substrate, employed to estimate the non-specific binding. This result suggests that, at the concentration of the substrate employed, non-saturable uptake in these cells was negligible. Conversely, MPP+ uptake in NCl-H441 cells was very low, although slightly increasing up to 30 min, and hardly inhibited by an excess of the substrate. In light of these results, we can conclude that A549 cells display the highest saturable uptake of MPP+, with Calu-3 following and NCl-H441 endowed with an only modest saturable uptake.

In addition, time-course of MPP+ uptake performed in polarized Calu-3 cells grown under air–liquid interface conditions (Calu-3 ALI), indicated that the accumulation of the substrate was linear up to 30 min and comparable when measured at the apical and basolateral side of the layers (Fig. 2, panel A). Under these conditions, the trans-cellular fluxes of MPP+ were detectable in both directions and quantitatively comparable from apical to basolateral side and *vice versa* (panel B).

3.2. Kinetic analysis of MPP+ uptake

Initial rates of transport were determined in the three cell lines over a wide range of MPP+ concentrations (from 0.8 to 1850 μM), both in the presence and in the absence of sodium (Fig. 3). Data obtained under the two experimental conditions were overlapping, thus

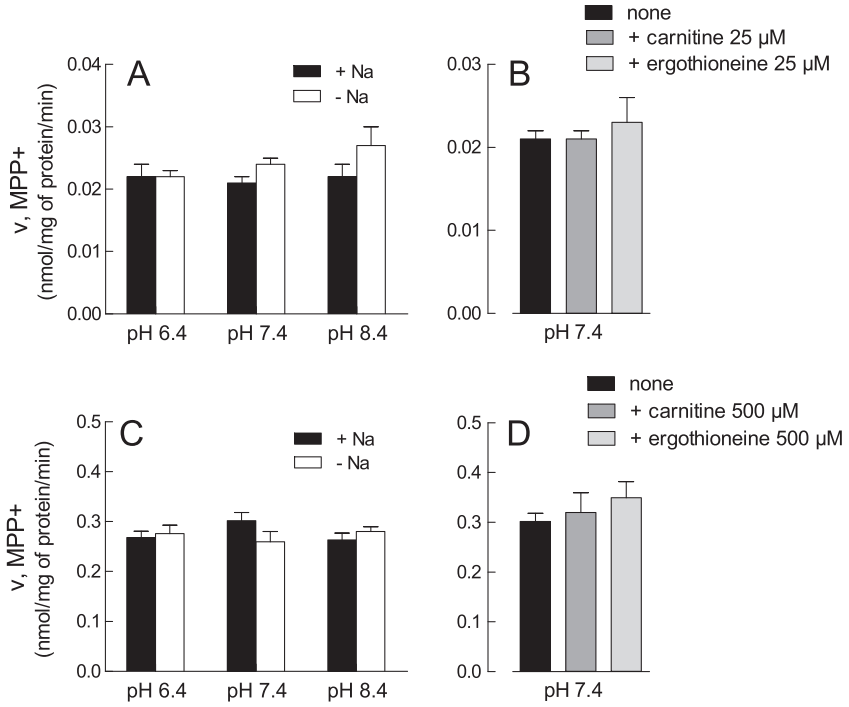

Fig. 8. Effect of pH on MPP+ uptake in Calu-3 cells. Cells were incubated for 10 min in the transport buffer containing 5 μM (panels A and B) or 100 μM (panels C and D) [^{3}H]MPP+ (2 μCi/ml) in the presence or in the absence of sodium (panels A and C) or in the presence of sodium (panels B and D) at the indicated pH. Carnitine or ergothioneine was added to the transport buffer as indicated (panels B and D). Each point represents the mean ± S.D. of four independent determinations. The experiment has been repeated twice with comparable results.

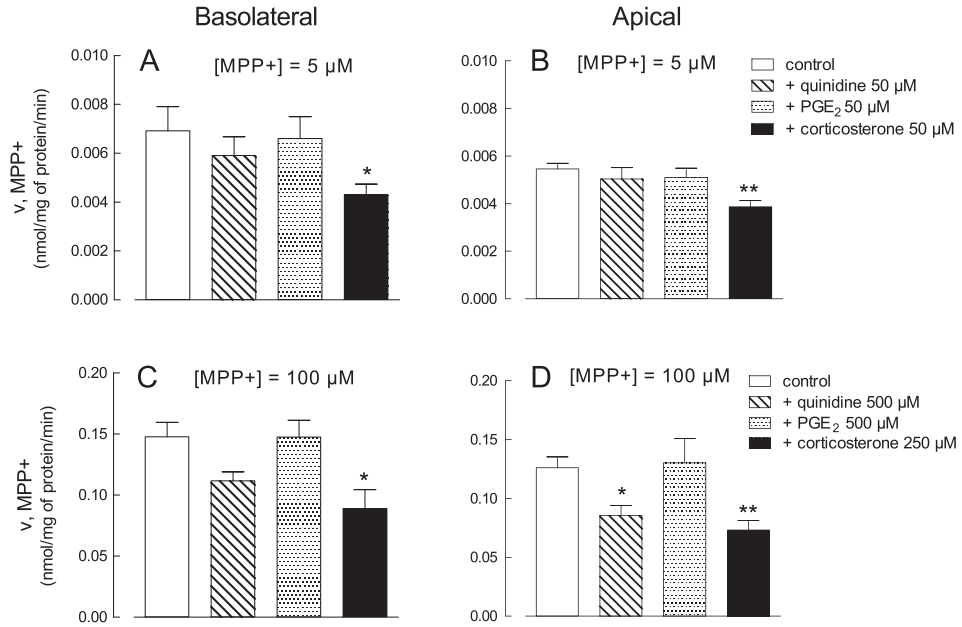

Fig. 9. Inhibition of MPP+ uptake in Calu-3 ALI. Polarized cells were maintained under air–liquid interface growth conditions (21 d). Apical and basolateral side were incubated for 10 min in the transport buffer containing 5 μM (panels A and B) or 100 μM (panels C and D) [^{3}H]MPP+ (2 μCi/ml) in the absence (control) or in the presence of the indicated concentrations of the inhibitors. Bars represent the mean ± S.D. of three independent determinations. The experiment has been repeated twice with comparable results. $^*p < 0.05$, $^{**}p < 0.01$ vs control.

demonstrating the complete Na^+-independence of MPP+ uptake in all cell models. Transport values in A549 cells were best fitted by Eq. (1) (see section Material and methods) and the resulting kinetic parameters revealed the presence of a high-affinity transport system plus diffusion (K_m about 50 μM with a V_{max} of about 1.5 nmol/mg of protein). Consistently, the Eadie–Hofstee plot of the saturable component (insert) was linear, confirming the operation of a single OCT transporter in this model. Also in NCI-H441 cells, transport data were best fitted by Eq. (1) but in this case the K_m values were higher (about 180 μM) and V_{max} values about ten times lower than in A549. On the contrary, in Calu-3 cells, MPP+ transport data were best fitted by Eq. (2), revealing the presence of at least two saturable transport components, one displaying a high-affinity for the substrate ($K_m \leq 20$ μM) and the other with a low-affinity ($K_m \geq 0.6$ mM). Accordingly, the regression analysis of the Eadie–Hofstee plot for the saturable MPP+ uptake in these cells (insert) appeared nonlinear, confirming the involvement of at least two different transporters.

A complete description of the apparent kinetic parameters obtained in the cell models is shown in Table 1.

3.3. Inhibition analysis of MPP+ uptake

In order to identify the contribution of each OCT to the transport of MPP+ in the three cell models, the uptake of the substrate was measured in the presence of increasing concentrations of the inhibitors quinidine, prostaglandin E_2 (PGE_2) and corticosterone [5]. In A549 cells both quinidine (Fig. 4, panel A), inhibitor of OCT1 [10], and PGE_2 (panel B), which preferentially inhibits OCT2 [5], were completely ineffective. On the contrary, the addition of corticosterone (panel C), which can inhibit all OCTs, but has a much higher affinity for OCT3 [5], was able to significantly reduce the uptake of 5 μM MPP+ in a concentration-dependent manner ($I_{0.5} = 1.29$ μM; maximal inhibition > 90%). From these data, the calculated *Ki* was 1.17 μM, a value very close to IC_{50} of corticosterone for OCT3 [5]. Overall these results point to OCT3 as the main transporter for MPP+ in A549 cells, excluding the contribution of OCT1 and OCT2.

In NCI-H441 cells all the inhibitors were ineffective at the concentrations employed for A549 (data not shown). Hence, the inhibition analysis has been performed at a higher concentration of MPP+ (50 μM) with

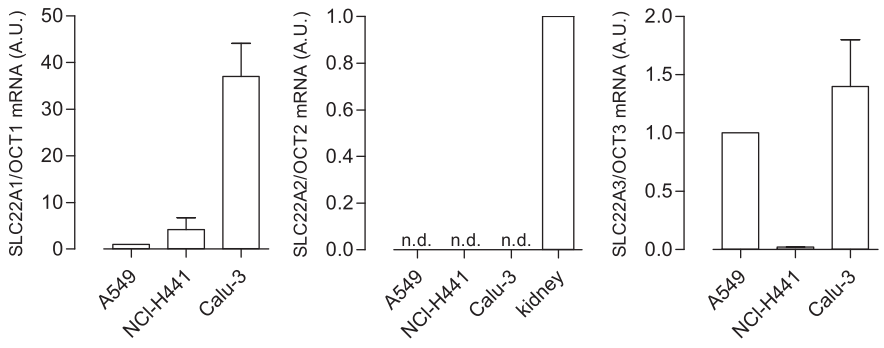

Fig. 10. Expression of OCT mRNA. mRNA levels for OCTs were determined through RT-qPCR analysis. After normalization to RPL-15, the expression of SLC22A1/OCT1, and SLC22A3/OCT3 in the different cell models was expressed relatively to that of A549 (=1). For SLC22A2/OCT2, cDNA obtained from human kidney was employed as positive control and set =1. Data are means ± S.E. of three experiments, each performed in duplicate.

increased concentrations of inhibitors (250 μM). The results, presented in Fig. 5, demonstrate that only quinidine modestly although significantly inhibited MPP+ uptake, with a maximal inhibition of about 30%. This finding points to OCT1 as the main transporter active in NCl-H441 cells.

Due to the operation of different transport components in Calu-3 cells, the inhibition analysis in these cells had to be performed at different concentrations of substrate, so as to properly identify the high and low affinity components. To choose the proper experimental conditions, the relative contribution of the high and low affinity components to total MPP+ uptake has been calculated at different concentrations of substrate, taking advantage of the proper kinetic parameters reported in Table 1. As shown in Fig. 6 the contribution of the high affinity transporter was prevalent at low concentrations of substrate (up to 10 μM), while the low affinity activity accounted for more than 60% at MPP+ > 100 μM. The effect of OCT inhibitors in Calu-3 has been hence assessed at both 5 and 100 μM MPP+ (Fig. 7). At 5 μM MPP+ (left panel), both corticosterone and quinidine inhibited the uptake, although to a different extent (maximal inhibition of about 80% for corticosterone and 50% for quinidine). $I_{0.5}$ values were in the order of micromolar (1.038 and 3.98 μM for corticosterone and quinidine, respectively). At 100 μM MPP+ (right panel), a concentration of substrate that better highlights the low affinity transport component, the percent of maximal inhibition obtained by quinidine increased, while that of corticosterone concomitantly decreased. PGE_2 was always ineffective. The results obtained from the inhibition analysis suggest that both OCT1 and OCT3 are active in Calu-3 cells. In order to exclude the involvement of other transporters such as OCTN1/2 and MATE1, the uptake of MPP+ was measured (Fig. 8) at both low (5 μM, panels A and B) and high (100 μM, panels C and D) concentrations of substrate, both in the presence and in the absence of sodium, employing transport buffer solutions at different pH (6.4, 7.4 and 8.4). Data obtained show that MPP+ uptake was pH-independent and sodium-independent at any value of pH, both at low and high substrate concentrations, thus excluding the contribution of MATE1, which is pH-dependent [24]. Moreover, carnitine and ergothioneine, the substrates of OCTN2 and OCTN1, respectively [25,26], did not inhibit MPP+ uptake (panels B and D). We thus conclude that in Calu-3 cells OCT3 represents the high affinity transporter for MPP+ while OCT1 accounts for the low affinity component.

The inhibition analysis on MPP+ transport has been, in addition, performed in polarized Calu-3 cells maintained under air–liquid interface grown conditions (Calu-3 ALI). The results, presented in Fig. 9, demonstrate that at 5 μM MPP+ only corticosterone significantly inhibited the uptake at both basolateral and apical sides, while quinidine and PGE_2 were ineffective (panels A and B). At 100 μM also quinidine, in addition to corticosterone, significantly inhibited MPP+ uptake at the apical side, while at the basolateral side only the inhibition by corticosterone was significant. In this latter condition PGE_2 was completely ineffective and quinidine caused a slight, not significant, inhibition (panels C and D). These results suggest that OCT3 is functional at both the basolateral and apical membranes in polarized Calu-3 cells, while a significant OCT1 activity is observed only at the apical side.

3.4. Expression of OCTs and MPP+ transport in silenced cells

Fig. 10 shows the expression of OCTs mRNA in A549, NCl-H441 and Calu-3 cells. The level of OCT1 was highest in Calu-3, with NCl-H441 following, and only barely detectable in A549. The expression of OCT2 was undetectable in all cell models while OCT3 was clearly evident in both A549 and Calu-3 cells but not in NCl-H441.

In light of these results, we next employed short interfering RNA (siRNA) to define the operation of OCT1 and OCT3 in A549 and Calu-3 cells. In A549 (Fig. 11), a significant, although incomplete, silencing of SLC22A3/OCT3 (about 40% compared with cells transfected with scrambled siRNA) was obtained after 96 h of incubation (panel A). The

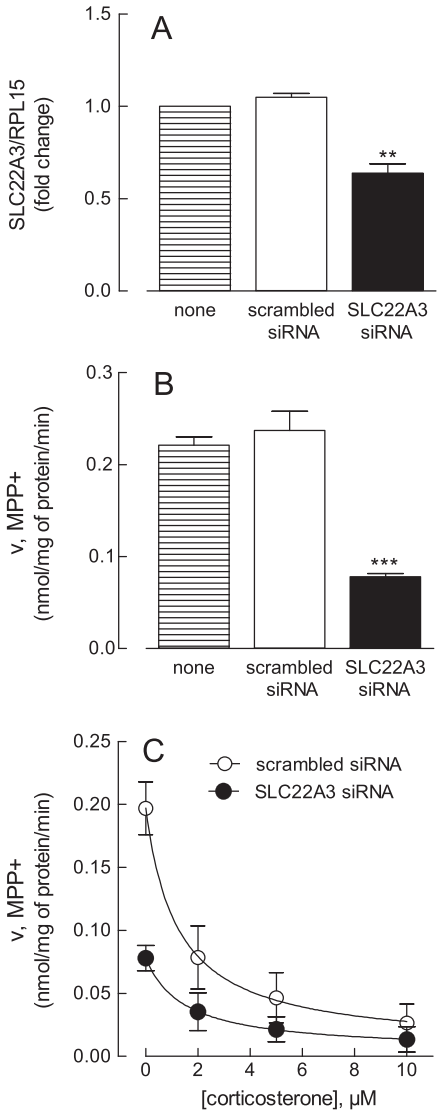

Fig. 11. SLC22A3/OCT3 silencing in A549 cells. A549 cells were transfected with scrambled or SLC22A3/OCT3 siRNA for 96 h, as described in Material and methods. Panel A. The expression of SLC22A3/OCT3 mRNA was assessed by qRT-PCR and shown relatively to that of untransfected cells (none = 1). Data are means ± S.E. of three separate determinations, each performed in duplicate. $^{**}p < 0.01$ vs untransfected cells (none). Panel B. The uptake of [^{3}H]MPP+ (5 μM; 2 μCi/ml; 5 min) was measured in cells untransfected (none) or transfected with scrambled or SLC22A3/OCT3 siRNA. Data are means ± S.E. of three independent experiments, each performed in quadruplicate. $^{***}p < 0.01$ vs scrambled siRNA. Panel C. Transfected cells were incubated for 5 min in the transport buffer containing [^{3}H]MPP+ (5 μM; 2 μCi/ml) with the indicated concentrations of corticosterone. Each point represents the mean ± S.D. of four independent determinations. Data were fitted by Eq. (3) (see section Material and methods). The experiment has been repeated twice with comparable results.

observed changes of gene expression were associated with a marked reduction of transport activity (>60%, panel B) in SLC22A3/OCT3 siRNA transfected cells. In this latter condition, the corticosterone-inhibitable fraction appeared much smaller compared to that observed in cells transfected with scrambled siRNA (panel C). The silencing of SLC22A1/OCT1 in this cell model was completely ineffective (result not shown). These results, besides confirming the prevalent operation of OCT3 in A549 cells, also validate the efficacy of corticosterone as OCT3 inhibitor. Fig. 12 shows the effect of SLC22A1/OCT1 and SLC22A3/OCT3 silencing on MPP+ transport activity in Calu-3 cells. As expected, OCT1 and OCT3 siRNA were specifically effective in reducing the expression of SLC22A1 (panel A) and SLC22A3 (panel B), respectively. The reduction was about 50% for both genes. The consequence of gene silencing on

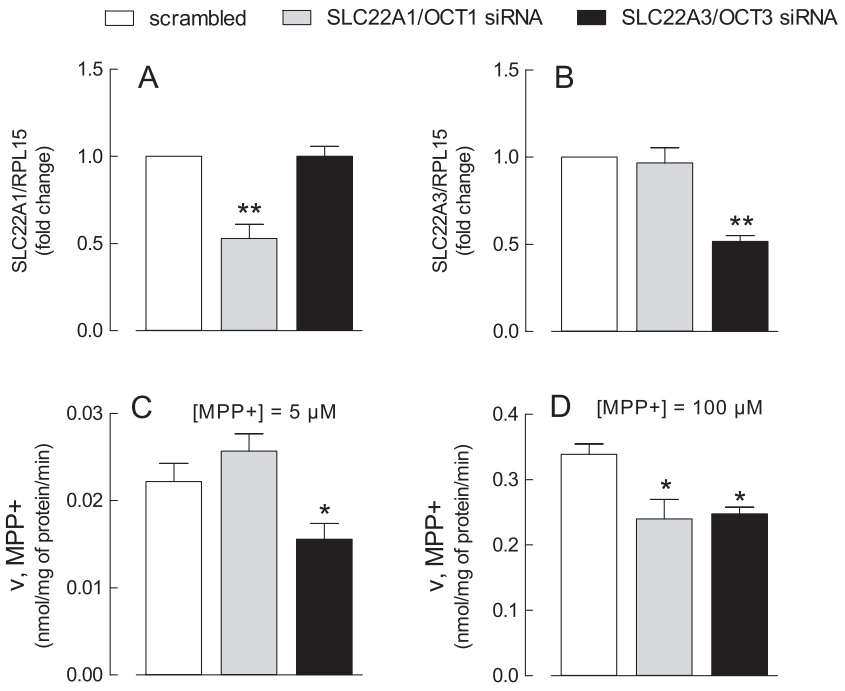

Fig. 12. SLC22A1/OCT1 and SLC22A3/OCT3 silencing in Calu-3 cells. Calu-3 cells were transfected with scrambled, SLC22A1/OCT1 or SLC22A3/OCT3 siRNA for 96 h, as described in Material and methods. Panels A and B. Relative expression of SLC22A1/OCT1 and SLC22A3/OCT3 mRNA assessed by qRT-PCR and shown relatively to that of scrambled transfected cells (=1). Data are means ± S.E. of three separate determinations, each performed in duplicate. $^{**}p < 0.01$ vs scrambled transfected cells. Panels B and C. The uptake of [^{3}H]MPP+ at 5 μM (panel C) or 100 μM (panel D) was measured. Data are means ± S.E. of two independent experiments, each performed in quadruplicate. $^{*}p < 0.05$ vs scrambled siRNA.

MPP+ transport was then evaluated by measuring substrate uptake at 5 μM (panel C) and 100 μM (panel D) MPP+. At 5 μM, only OCT3 silencing caused a significant reduction of MPP+ transport while OCT1 silencing was ineffective. At 100 μM MPP+ both OCT1 and OCT3 siRNA caused a modest (about 30%) although significant inhibition of the transport. These results confirm the contribution of both OCT1 and OCT3 to MPP+ transport in Calu-3 cells.

3.5. Characterization of MPP+ transport in bronchial BEAS-2B epithelial cells

The characterization of MPP+ transport has been performed also in a model of immortalized epithelial cells derived from normal lung (BEAS-2B). Panel A of Fig. 13 shows that also in these cells MPP+ transport is saturable and almost linear for 60 min. Kinetic analysis performed both in the absence and in the presence of extracellular sodium revealed the presence of at least two saturable transport components, one displaying a very high-affinity for the substrate ($K_m \leq 1$ μM) and the other with a lower affinity (K_m of ~0.1 mM). Both components are endowed with fairly low values of V_{max} (0.0025 and 0.045 nmol/mg of protein/min, respectively). The inhibition analysis has been, hence, performed at two different concentration of MPP+, so as to properly identify these components. Both at 1 μM (panel C) and 50 μM (panel D) MPP+ corticosterone and quinidine significantly inhibited MPP+ transport, with a higher effect of corticosterone at the lowest concentration and a predominant effect of quinidine at 50 μM MPP+. PGE_2 was ineffective. These results point to OCT3 and OCT1 as transporters for MPP+ in BEAS-2B cells.

4. Discussion

The aim of the present study was to define the functional activity and the expression of organic cation transporters (OCTs) in *in vitro* pulmonary cell models, that could ultimately be employed for studies concerning drug transportation in the lung. In this context, clear-cut differences have been highlighted at functional level among the considered human airway epithelial cell models. In particular, A549 cells appear the ones displaying the more sustained uptake of MPP+, which is mediated by a single high-affinity transporter, as indicated by the results of the kinetic analysis (see Fig. 3). The inhibition analysis of MPP+ uptake reveals the efficacy of the sole corticosterone, with a *Ki* value consistent with the affinity of corticosterone for OCT3 [5]. Moreover the use of specific siRNA targeting SLC22A3/OCT3 confirms that this is the transporter functionally operative in MPP+ uptake in A549 cells. In support of functional data, mRNA expression shows that only OCT3 is clearly expressed in these cells. Our results are in line with previous findings by other groups [27,28], while different conclusions have been reached by Salomon *et al.* when addressing OCT transport activity employing the fluorescent organic cation 4-(4-(dimethylamino)styryl)-N-methylpyridinium iodide (Asp+) as substrate [16]. The authors stated, indeed, that Asp+ uptake was higher in A549 than in other cell types (Calu-3, 16HBE14o- and Caco-2 cells), a result in agreement with our data with MPP+; however, their kinetic analysis indicated the involvement of two different transport components, and both OCT2 and, probably, OCT3 were found active in these cells. We can presume that these discrepancies are likely due to a different specificity of MPP+ and Asp+ towards OCTs, since the first is a specific substrate of OCTs, while different transporters, such as OCTN, may be involved in Asp+ uptake, as demonstrated by the same authors [16].

Data obtained in Calu-3 cells point, instead, to the involvement of more than one transporter in MPP+ uptake. Kinetic analysis indicates the contribution of two saturable components to total uptake, with a high ($K_m < 20$ μM) and a low ($K_m > 0.6$ mM) affinity for the substrate. The elaboration of the kinetic parameters allowed us to estimate the relative contribution of the two transport components at any concentration of substrate (see Fig. 6), that in turn enabled the selection of the optimal discriminating conditions for the inhibition analysis: at low concentrations of MPP+, the contribution of the high affinity component appears largely predominant, and the inhibition by corticosterone identifies OCT3 as the high affinity transporter (see Fig. 7, left). Conversely, when MPP+ transport is measured at higher concentration (100 μM), where the low affinity component becomes predominant,

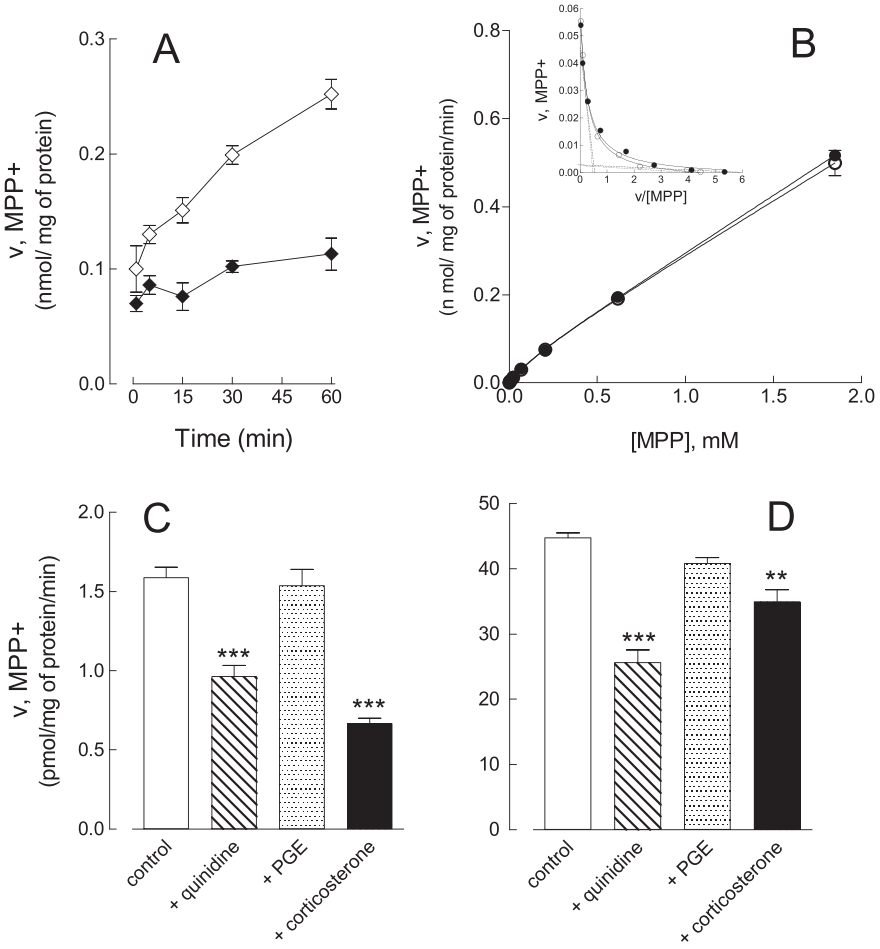

Fig. 13. Characterization of MPP+ uptake in BEAS-2B cells. Panel A. BEAS-2B cells were incubated for the indicated times in the transport buffer (see Material and methods) containing [^{3}H]MPP+ (10 μM; 2 μCi/ml) (open symbols). Non-specific binding of the substrate was estimated by measuring [^{3}H]MPP+ uptake in the presence of an excess of unlabelled substrate (2 mM, filled symbols). Each point represents the mean ± S.D. of four independent determinations. Panel B. Cells were incubated in the presence of the indicated concentrations (from 0.8 to 1850 μM) of [^{3}H]MPP+ (2 μCi/ml) for 15 min in the absence (open symbols) or in the presence (filled symbols) of Na^+. Nonlinear fitting of the data was performed employing Eq. (2) (see Material and methods). Insert shows the Eadie–Hofstee transformations of the saturable uptake (obtained after subtraction of the diffusive component estimated by the nonlinear fitting). Curves represent the nonlinear fitting of the data. Straight lines are drawn employing the values of the kinetic parameters given by nonlinear regression. Points are mean ± S.D. of three independent determinations. The experiment has been repeated twice with comparable results. Panels C and D. Cells were incubated for 15 min in the transport buffer containing 1 μM (panel C) or 50 μM (panel D) [^{3}H]MPP+ (2 μCi/ml) in the presence of the indicated concentrations of the inhibitors. Each point represents the mean ± S.D. of four independent determinations. The experiment has been repeated three times with comparable results.

the inhibition by quinidine increases, pointing to OCT1 as the low affinity transporter (see Fig. 7, right). The use of specific siRNA confirmed these findings (see Fig. 12). mRNA expression (see Fig. 10) excludes the presence of OCT2 in these cells, in line with previous observations by other groups [16,29,30]. Moreover, the pH-independency and the lack of inhibition of carnitine and ergothioneine on MPP+ transport, allow excluding the contribution of MATE1 and OCTNs to the transport of MPP+ in this cell model. We conclude that OCT1 and OCT3 are the ones functionally active in Calu-3, both when unpolarized (*i.e.* grown on plasticware) and polarized (*i.e.* grown under air–liquid interface condition, ALI). As far as this latter condition is concerned, we next addressed the cellular localization of the transporters, basolateral rather than apical, an issue, thus far, only roughly defined. To this concern, permeation approaches performed by Mukherjee *et al.*, by employing Asp+ as substrate, suggested the presence of an OCT activity only at the apical side of Calu-3 cells; since the dye was not significantly transported across the monolayers from the apical into the basolateral compartment of the transwell chambers, they excluded OCT activity at the basolateral side of the cells [30]. Conversely, a similar study by MacDonald *et al.* showed that Asp+ is not only actively taken up at both sides of the cells, but it is also transported across the monolayer with a flux from apical versus basolateral significantly higher than the opposite [29]. Accordingly, our results in Calu-3 ALI indicate a bi-directional transfer of MPP+ into the opposite compartment, which is mediated by both OCT1 and OCT3 at the apical and by OCT3 at the basolateral side of the monolayer.

As far as NCl-H441 cells are concerned, results obtained appear peculiar, since only OCT1 is expressed and a very modest saturable uptake of MPP+ is measurable. Accordingly, results of the kinetic analysis clearly indicate that MPP+ uptake is mediated by a single saturable component endowed with a relatively high affinity (K_m = 180 μM) and a very low value of V_{max} (about ten times lower than that measured in A549 cells). The transport activity could be, hence, ascribed to a non-saturable, rather than to an active component; however, the modest, but significant, inhibitory effect of quinidine and the lack of inhibition by corticosterone and PGE_2 confirm that OCT1 is responsible of MPP+ uptake in NCl-H441 cells. Recently, Salomon *et al.* reported a K_m in the similar order of magnitude (881.2 ± 195.3 μM) and a V_{max} much higher than our (2.07 ± 0.26 nmol/min/mg protein) for Asp+ uptake [20]. Whether these differences could be explained by the involvement of other transporters or by a different specificity of the two substrates employed remains to be established. Finally, we present here for the first time, a functional characterization of MPP+ transport in a model of immortalized human bronchial epithelial cells (BEAS-2B), a line of cells obtained from normal lung.

These cells exhibit an only modest saturable MPP+ transport with values comparable to that of NCI-H441. On the other hand, kinetic and inhibition analyses show a pattern of transport similar to that of Calu-3 cells. Further studies are necessary to ascertain whether differences among OCT activity in adenocarcinoma derived cell lines and normal cells actually exist and can be ascribed to the malignant phenotype.

5. Conclusions

Overall, these results are of particular relevance for the definition of the operative features of OCT transporters in organotypic *in vitro* models of human respiratory epithelium. Clear cut differences have been detected among the considered airway epithelial cells as far as OCT expression and activity are concerned. In particular A549 and NCI-H441 cells appear suitable models for the study of drug interaction with the sole OCT3 or OCT1, respectively. Conversely, the simultaneous contribution of OCT1 and OCT3 to cationic drug transport is appreciable in Calu-3 and BEAS-2B cells. All the cell models employed are unusable for studies of drug interaction with OCT2, due to its lack of expression. These findings could, thus, help to identify the proper *in vitro* model for researches of drug absorption and disposition.

Conflict of interest

The authors declare no competing financial interests.

Acknowledgments

This work was supported by Chiesi Farmaceutici, Parma, Italy (66DALLACHIESI).

References

[1] A. Ayrton, P. Morgan, Role of transport proteins in drug discovery and development: a pharmaceutical perspective, Xenobiotica 38 (2008) 676–708.
[2] H. Koepsell, H. Endou, The SLC22 drug transporter family, Pflugers Arch. 447 (2004) 666–676.
[3] H. Koepsell, The SLC22 family with transporters of organic cations, anions and zwitterions, Mol. Asp. Med. 34 (2013) 413–435.
[4] N. Longo, C. Amat di San Filippo, M. Pasquali, Disorders of carnitine transport and the carnitine cycle, Am. J. Med. Genet. C: Semin. Med. Genet. 142C (2006) 77–85.
[5] H. Koepsell, K. Lips, C. Volk, Polyspecific organic cation transporters: structure, function, physiological roles, and biopharmaceutical implications, Pharm. Res. 24 (2007) 1227–1251.
[6] J.W. Jonker, A.H. Schinkel, Pharmacological and physiological functions of the polyspecific organic cation transporters: OCT1, 2, and 3 (SLC22A1-3), J. Pharmacol. Exp. Ther. 308 (2004) 2–9.
[7] S.H. Wright, Role of organic cation transporters in the renal handling of therapeutic agents and xenobiotics, Toxicol. Appl. Pharmacol. 204 (2005) 309–319.
[8] W.M. Suhre, S. Ekins, C. Chang, P.W. Swaan, S.H. Wright, Molecular determinants of substrate/inhibitor binding to the human and rabbit renal organic cation transporters hOCT2 and rbOCT2, Mol. Pharmacol. 67 (2005) 1067–1077.
[9] M. Hayer-Zillgen, M. Bruss, H. Bonisch, Expression and pharmacological profile of the human organic cation transporters hOCT1, hOCT2 and hOCT3, Br. J. Pharmacol. 136 (2002) 829–836.
[10] A.T. Nies, H. Koepsell, K. Damme, M. Schwab, Organic cation transporters (OCTs, MATEs), in vitro and in vivo evidence for the importance in drug therapy, Handb. Exp. Pharmacol. (2011) 105–167.
[11] V. Gorboulev, J.C. Ulzheimer, A. Akhoundova, I. Ulzheimer-Teuber, U. Karbach, S. Quester, C. Baumann, F. Lang, A.E. Busch, H. Koepsell, Cloning and characterization of two human polyspecific organic cation transporters, DNA Cell Biol. 16 (1997) 871–881.
[12] K.S. Lips, C. Volk, B.M. Schmitt, U. Pfeil, P. Arndt, D. Miska, L. Ermert, W. Kummer, H. Koepsell, Polyspecific cation transporters mediate luminal release of acetylcholine from bronchial epithelium, Am. J. Respir. Cell Mol. Biol. 33 (2005) 79–88.
[13] L. Zhang, M.J. Dresser, A.T. Gray, S.C. Yost, S. Terashita, K.M. Giacomini, Cloning and functional expression of a human liver organic cation transporter, Mol. Pharmacol. 51 (1997) 913–921.
[14] C. Bosquillon, Drug transporters in the lung—do they play a role in the biopharmaceutics of inhaled drugs? J. Pharm. Sci. 99 (2010) 2240–2255.
[15] M. Gumbleton, G. Al-Jayyoussi, A. Crandon-Lewis, D. Francombe, K. Kreitmeyr, C.J. Morris, M.W. Smith, Spatial expression and functionality of drug transporters in the intact lung: objectives for further research, Adv. Drug Deliv. Rev. 63 (2011) 110–118.
[16] J.J. Salomon, S. Endter, G. Tachon, F. Falson, S.T. Buckley, C. Ehrhardt, Transport of the fluorescent organic cation 4-(4-(dimethylamino)styryl)-N-methylpyridinium iodide (ASP+) in human respiratory epithelial cells, Eur. J. Pharm. Biopharm. 81 (2012) 351–359.
[17] K. Bleasby, J.C. Castle, C.J. Roberts, C. Cheng, W.J. Bailey, J.F. Sina, A.V. Kulkarni, M.J. Hafey, R. Evers, J.M. Johnson, R.G. Ulrich, J.G. Slatter, Expression profiles of 50 xenobiotic transporter genes in humans and pre-clinical species: a resource for investigations into drug disposition, Xenobiotica 36 (2006) 963–988.
[18] S. Endter, D. Francombe, C. Ehrhardt, M. Gumbleton, RT-PCR analysis of ABC, SLC and SLCO drug transporters in human lung epithelial cell models, J. Pharm. Pharmacol. 61 (2009) 583–591.
[19] J.J. Salomon, C. Ehrhardt, Organic cation transporters in the blood–air barrier: expression and implications for pulmonary drug delivery, Ther. Deliv. 3 (2012) 735–747.
[20] J.J. Salomon, V.E. Muchitsch, J.C. Gausterer, E. Schwagerus, H. Huwer, N. Daum, C.M. Lehr, C. Ehrhardt, The cell line NCI-H441 is a useful in vitro model for transport studies of human distal lung epithelial barrier, Mol. Pharm. 11 (2014) 995–1006.
[21] M. Belzer, M. Morales, B. Jagadish, E.A. Mash, S.H. Wright, Substrate-dependent ligand inhibition of the human organic cation transporter OCT2, J. Pharmacol. Exp. Ther. 346 (2013) 300–310.
[22] A. Barilli, B.M. Rotoli, R. Visigalli, O. Bussolati, G.C. Gazzola, V. Dall'Asta, Arginine transport in human monocytic leukemia THP-1 cells during macrophage differentiation, J. Leukoc. Biol. 90 (2011) 293–303.
[23] G.C. Gazzola, V. Dall'Asta, R. Franchi-Gazzola, M.F. White, The cluster-tray method for rapid measurement of solute fluxes in adherent cultured cells, Anal. Biochem. 115 (1981) 368–374.
[24] M. Otsuka, T. Matsumoto, R. Morimoto, S. Arioka, H. Omote, Y. Moriyama, A human transporter protein that mediates the final excretion step for toxic organic cations, Proc. Natl. Acad. Sci. U. S. A. 102 (2005) 17923–17928.
[25] D. Grundemann, S. Harlfinger, S. Golz, A. Geerts, A. Lazar, R. Berkels, N. Jung, A. Rubbert, E. Schomig, Discovery of the ergothioneine transporter, Proc. Natl. Acad. Sci. U. S. A. 102 (2005) 5256–5261.
[26] I. Tamai, R. Ohashi, J. Nezu, H. Yabuuchi, A. Oku, M. Shimane, Y. Sai, A. Tsuji, Molecular and functional identification of sodium ion-dependent, high affinity human carnitine transporter OCTN2, J. Biol. Chem. 273 (1998) 20378–20382.
[27] N. Ishiguro, M. Oyabu, T. Sato, T. Maeda, H. Minami, I. Tamai, Decreased biosynthesis of lung surfactant constituent phosphatidylcholine due to inhibition of choline transporter by gefitinib in lung alveolar cells, Pharm. Res. 25 (2008) 417–427.
[28] T. Wang, J. Li, F. Chen, Y. Zhao, X. He, D. Wan, J. Gu, Choline transporters in human lung adenocarcinoma: expression and functional implications, Acta Biochim. Biophys. Sin. (Shanghai) 39 (2007) 668–674.
[29] C. Macdonald, D. Shao, A. Oli, R.U. Agu, Characterization of Calu-3 cell monolayers as a model of bronchial epithelial transport: organic cation interaction studies, J. Drug Target. 21 (2013) 97–106.
[30] M. Mukherjee, D.I. Pritchard, C. Bosquillon, Evaluation of air-interfaced Calu-3 cell layers for investigation of inhaled drug interactions with organic cation transporters in vitro, Int. J. Pharm. 426 (2012) 7–14.